Available online at www.sciencedirect.com
ScienceDirect
Trans. Nonferrous Met. Soc. China 34(2024) 2415−2430
Transactions of Nonferrous Metals Society of China
www.tnmsc.cn

Effect of interrupted aging on mechanical properties and corrosion resistance of 7A75 aluminum alloy

Xian-wen YANG[1], Ling-ying YE[1], Yong ZHANG[1], Quan-shi CHENG[1,2]

1. School of Materials Science and Engineering, Central South University, Changsha 410083, China;
2. Aerospace Precision Production Co., Ltd., Tianjin 300300, China

Received 23 February 2023; accepted 5 September 2023

Abstract: The effects of interrupted aging on mechanical properties and corrosion resistance of 7A75 aluminum alloy extruded bar were investigated through various analyses, including electrical conductivity, mechanical properties, local corrosion properties, and slow strain rate tensile stress corrosion tests. Microstructure characterization techniques such as metallographic microscopy, scanning electron microscopy (SEM), and transmission electron microscopy (TEM) were also employed. The results indicate that the tensile strength of the alloy produced by T6I6 aging is similar to that produced by T6I4 aging, and it even exceeds 700 MPa. Furthermore, the yield strength increases by 52.7 MPa, reaching 654.8 MPa after T6I6 aging treatment. The maximum depths of intergranular corrosion (IGC) and exfoliation corrosion (EXCO) decrease from 116.3 and 468.5 μm to 89.5 and 324.3 μm, respectively. The stress corrosion factor also decreases from 2.1% to 1.6%. These findings suggest that the alloy treated with T6I6 aging exhibits both high strength and excellent stress corrosion cracking resistance. Similarly, when the alloy is treated with T6I4, T6I6 and T6I7 aging, the sizes of grain boundary precipitates (GBPs) are found to be 5.2, 18.4, and 32.8 nm, respectively. The sizes of matrix precipitates are 4.8, 5.7 and 15.7 nm, respectively. The atomic fractions of Zn in GBPs are 9.92 at.%, 8.23 at.% and 6.87 at.%, respectively, while the atomic fractions of Mg are 12.66 at.%, 8.43 at.% and 7.00 at.%, respectively. Additionally, the atomic fractions of Cu are 1.83 at.%, 2.47 at.% and 3.41 at.%, respectively.

Key words: 7A75 aluminum alloy; interrupted aging; aging precipitation behavior; mechanical properties; intergranular corrosion; exfoliation corrosion; stress corrosion cracking

1 Introduction

Precipitation-strengthenable Al−Zn−Mg−Cu alloys are extensively applied as crucial structural materials in the transportation industry to decrease component mass [1,2]. The excellent mechanical properties of the alloys, particularly their high specific strength, make them highly sought-after for diverse applications [3,4]. However, Al−Zn−Mg−Cu alloys are susceptible to various forms of corrosion, including intergranular corrosion (IGC), exfoliation corrosion (EXCO) and stress corrosion cracking (SCC). Consequently, achieving a balance between mechanical properties and corrosion resistance has emerged as a significant area of research.

The properties of Al−Zn−Mg−Cu alloys, particularly the mechanical properties and corrosion resistance, are primarily influenced by the precipitation behavior during aging processes [5]. The precipitation sequence of Al−Zn−Mg−Cu alloys is as follows: supersaturated solid solution → GP (I, II) zones → η' precipitates → η precipitates [6]. In general, the primary strengthening precipitates during the aging processes are the coherent GP (I, II) zones and semi-coherent η' precipitates [2−7]. However, a prolonged aging time can lead to the

Corresponding author: Ling-ying YE, Tel: +86-13607435545, E-mail: lingyingye@csu.edu.cn
DOI: 10.1016/S1003-6326(24)66550-7

formation of non-coherent η precipitates within the matrix, which can reduce the intensity of the alloys [8]. Additionally, the stable η precipitates with different morphologies and distributions tend to form along the grain boundaries, significantly affecting the corrosion resistance of alloys [9,10]. It is well known that Al−Zn−Mg−Cu alloys can achieve the highest strength after T6 aging treatment, but they are more susceptible to various forms of corrosion [2,11,12]. The T7X and other over-aged states can effectively improve the corrosion resistance of the alloys but at the cost of 10%−15% loss in strength [2,13,14]. To overcome the problems of precipitation-free zones (PFZs) and improve the mechanical properties of the alloys, a new aging treatment, interrupted aging, has been proposed recently. Interrupted aging has been widely used in 2XXX series aluminum alloys, and Al−Zn−Mg−Cu alloys have also adopted this aging treatment to gradually improve their comprehensive properties. JACUMASSO et al [15] found that 7050 aluminum alloy can obtain higher precipitate phase density and better mechanical properties through T6I4 aging treatment, which involves 485 °C solution heat treatment for 4 h, 130 °C for 30 min, and 65 °C for 24 h. ANTUNES et al [16] found that the tensile strength of 7050 aluminum alloy can reach 561.0 MPa via T6I4 aging, which involves solution heat treatment at 485 °C for 4 h followed by artificial aging at 145 °C for 30 min and 65 °C for 24 h. Similarly, 7075 aluminum alloy also adopts this aging treatment to improve its mechanical properties. LI et al [17] found that the tensile strength of 7075 aluminum alloy sheet with 2 mm in thickness can reach 563.0 MPa via T6I6 process, which involves heat treatment at 470 °C for 1 h, 130 °C for 80 min, 65 °C for 240 h and 130 °C for 18 h, but the corrosion resistance becomes worse than that achieved by T73 aging treatment. KACZMAREK et al [18] found that the yield strength of 7075 aluminum alloy can reach 460.0 MPa and 520.0 MPa respectively by means of T6I4 and T6I6 aging processes after solution heat treatment at 540 °C. It is evident that the interrupted aging treatment strongly affects the mechanical properties and corrosion resistance of aluminum alloys. However, the effects of interrupted aging on the comprehensive properties and the mechanisms of 7A75 aluminum alloy extruded bar have not been systematically studied, and the further exploration and summary are urgently needed.

In this study, the effects of T6I4, T6I6 and T6I7 aging treatments on the mechanical properties and corrosion resistance of 7A75 aluminum alloy extruded bar were investigated. The objective is to enhance both the mechanical properties and corrosion resistance of the alloy. Various interrupted aging processes were examined, and their impacts on mechanical properties and corrosion resistance of the alloy were analyzed and discussed in relation to the microstructure. The findings of this study contribute to our understanding of the relationship between mechanical properties and corrosion resistance of 7A75 aluminum alloy extruded bar produced through different interrupted aging treatments. Additionally, these results offer valuable insights for achieving high comprehensive properties in the 7A75 aluminum alloy extruded bar.

2 Experimental

2.1 Materials and treatments

The raw material utilized in this study is 7A75 aluminum alloy extruded bar with a diameter of 12 mm, which underwent T6 aging treatment. The chemical composition of the alloy is presented in Table 1. The two-stage solid solution treatment involved heating the bars to 450 °C for 1 h, followed by heating them to 490 °C for 1 h. Initially, the bars were held at 450 °C for 1 h and then rapidly heated to 490 °C within 5 min. Subsequently, the bars were maintained at 490 °C for 1 h in the furnace and then quenched in water to bring them back to room temperature. After this, the aging process involved heating the bars to 121 °C for 2 h. Finally, the bars were held at a relatively low temperature for long insulation followed by re-aging treatment. After each step, the bars were water-quenched to room temperature. The parameters for the aging treatments are listed in Table 2.

Table 1 Chemical composition of 7A75 aluminum alloy (wt.%)

Zn	Mg	Cu	Mn	Cr
5.82	2.63	1.68	0.02	0.20
Ni	Ti	Fe	Si	Al
0.01	0.02	0.16	0.06	Bal.

Table 2 Interrupted aging conditions of 7A75 aluminum alloy

Aging treatment	Solid solution treatment	Pre-aging	Interrupted aging	Re-aging
T6I4	(450 °C, 1 h) + (490 °C, 1 h)	121 °C, 2 h	65 °C, 7 d	−
T6I6	(450 °C, 1 h) + (490 °C, 1 h)	121 °C, 2 h	65 °C, 7 d	121 °C, 16 h
T6I7	(450 °C, 1 h) + (490 °C, 1 h)	121 °C, 2 h	65 °C, 7 d	177 °C, 16 h

2.2 Properties test and microstructure observation

The samples used for the hardness and electrical conductivity tests were obtained from the same area. A 10 mm cylinder was intercepted along the extrusion direction, and the surface to be tested was smoothed and flattened prior to the test. The VH1202 Knoop/Vickers hardness tester was used for hardness test with a loading load of 19.6 N and a loading time of 15 s to measure hardness. The Fischer SMP 350 electrical conductivity tester was used for the electrical conductivity test. The average values of five data points for hardness and electrical conductivity were considered as the effective results.

For the room-temperature tensile test, parallel sections of the samples with a diameter of 8 mm and a length of 40 mm were marked. After undergoing the corresponding aging processes, the samples were tested using the MTS landmark 100 kN testing machine at a tensile rate of 2 mm/min. The average value of three samples from the same group was taken as the effective result of the experiment.

Transmission electron microscopy (TEM) observation was conducted using the FEI-Tecnaig20 TEM with an accelerated voltage of 200 kV. The preparation process for TEM samples involved machining the sample into a thin slice with a thickness of approximately 80 μm. The thin slice was then punched into disks with a diameter of 3 mm. Finally, the RL-2 electrolytic polishing twin-jet unit was used to thin the samples at a temperature of around −30 °C and a voltage of 20 V. The electrolytic solution composition consisted of 30% HNO_3 and 70% CH_3OH (in volume fraction).

For the slow strain rate tensile test, parallel sections of samples with a diameter of 6 mm and a length of 30 mm were tested using the YYF-100 slow strain rate stress corrosion testing machine at a strain rate of 1×10^{-6} s^{-1}. The samples were tested in a 50 °C, 3.5 wt.% NaCl solution and a 50 °C silicone oil, respectively. The average values of three samples from the same group were considered as the effective result of the experiment.

3 Result

3.1 Electrical conductivity and mechanical properties

The electrical conductivity and mechanical properties of 7A75 aluminum alloy treated with different interrupted aging processes are summarized in Table 3. As can be seen, when the alloy is treated with T6I4 aging process, the hardness and electrical conductivity of the alloy reach HV 183.5 and 27.3% (IACS), respectively. The ultimate tensile strength (UTS) and yield strength (YS) are 701.8 MPa and 602.1 MPa, respectively. After T6I6 aging treatment, the hardness and electrical conductivity of the alloy increase to HV 192.3 and 28.5% (IACS), respectively. The tensile strength remains unchanged at 704.4 MPa, but the yield strength increases by 52.7 to 654.8 MPa, representing an increase rate of 8.8% compared to T6I4 aging treatment. Compared to T6I4 aging temper, the hardness, electrical conductivity and strength of the alloy undergo significant changes after the T6I7 aging process. Specifically, the hardness decreases by HV 21.7 (11.9%) to HV 161.8, while the electrical conductivity increases to 36.3% (IACS) with an increment of 9.0%. The tensile strength and yield strength decrease to 552.4 MPa and 490.4 MPa, respectively, representing a decrease of 149.4 MPa (21.3%) and 111.7 MPa (18.6%), respectively. The elongations (σ) after the three aging treatments are 13.6%, 12.9% and 12.3%, respectively, which basically have not changed significantly. The yield ratio, which is the ratio of the yield strength to the tensile strength of the alloy, can reflect the toughness level of the alloy to some extent. The values of the alloy are 0.86, 0.93 and 0.89 when subjected to T6I4, T6I6 and T6I7 aging processes, respectively.

3.2 Precipitation behavior

Figure 1 displays the TEM bright field images of grain boundary precipitates (GBPs) in 7A75 aluminum alloy, treated with different interrupted aging methods. In Fig. 1(a), the SADE patterns along the $\langle 110\rangle_{Al}$ direction reveal the clear formation of GP (I, II) zones. These zones are coherent precipitates with the matrix which form during the initial stages of natural aging or artificial aging treatment [8,19]. Semi-coherent η' precipitates can be observed at the visible diffraction spots located at 1/3 {220} and 2/3 {220} positions [20]. GP (I, II) zones and η' precipitates are the primary strengthening precipitation phases in this alloy. The presence of diffraction spots near the {220} position of 2/3 indicates the formation of non-coherent η precipitates with larger particle sizes, which can reduce the strength of the alloy to some extent [21]. When the alloy is subjected to T6I4 aging, fine and continuous precipitates are distributed along the grain boundaries, with the width of PFZs measuring 10.6 nm and the size of GBPs measuring 8.2 nm, respectively (Fig. 1(b)). Under the T6I6 aging treatment, fine precipitates are still present along the grain boundaries, but the degree of continuity is reduced. The width of PFZs and the size of GBPs increase to 25.1 and 18.4 nm, respectively (Fig. 1(c)). When the aging treatment

Table 3 Electrical conductivity and mechanical properties of 7A75 aluminum alloy treated by different interrupted aging processes

Aging treatment	Hardness (HV)	Electrical conductivity/% (IACS)	UTS/MPa	YS/MPa	δ/%	Yield ratio
T6I4	183.5±2.1	27.3±0.1	701.8±1.2	602.1±1.0	13.6±0.1	0.86±0.05
T6I6	192.3±1.8	28.5±0.1	704.4±6.0	654.8±5.2	12.9±0.1	0.93±0.05
T6I7	161.8±2.0	36.3±0.2	552.4±3.1	490.4±2.7	12.3±0.1	0.89±0.05

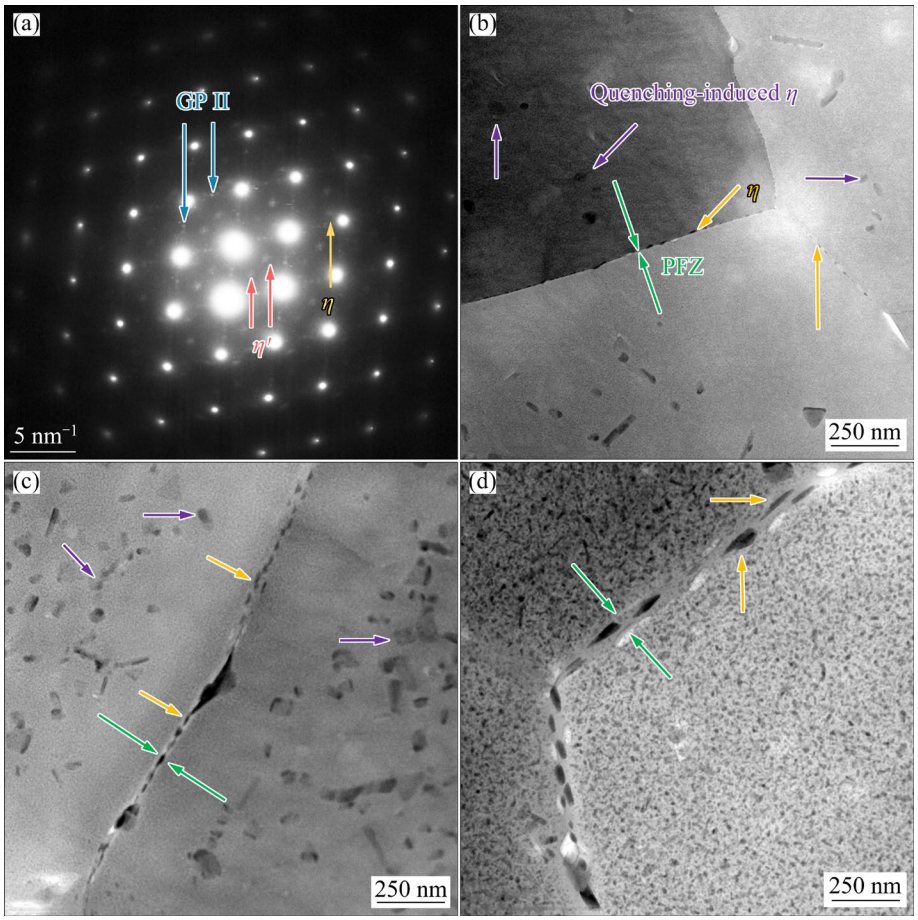

Fig. 1 Bright field TEM images at and around GBPs of 7A75 aluminum alloy: (a) SAED of samples near ⟨110⟩ direction; (b) T6I4; (c) T6I6; (d) T6I7

is changed to T6I7, the grain boundary morphologies of the alloy undergo significant changes. The PFZs widen noticeably, and the size of GBPs further increases. Additionally, the spaces between GBPs become wider and wider. The width of PFZs and the dimension of GBPs are 76.7 and 32.8 nm, respectively (Fig. 1(d)).

Figure 2 displays the TEM bright field images of matrix precipitates (MPs) in 7A75 aluminum alloy, which were treated using different interrupted aging processes. The morphologies of the MPs in the samples treated with T6I4 and T6I6 aging processes show minimal differences. In the matrix, a few coarse rod-like and irregular precipitates can be observed, while other fine and dispersed second phases are evenly distributed throughout the alloy. According to the report of LIU et al [22], these coarse particles are known as the quenching-induced η precipitates, which form when the supersaturated solid solution decomposes due to insufficient cooling rate during solid solution treatment. The sizes of the MPs are 4.8 and 5.7 nm

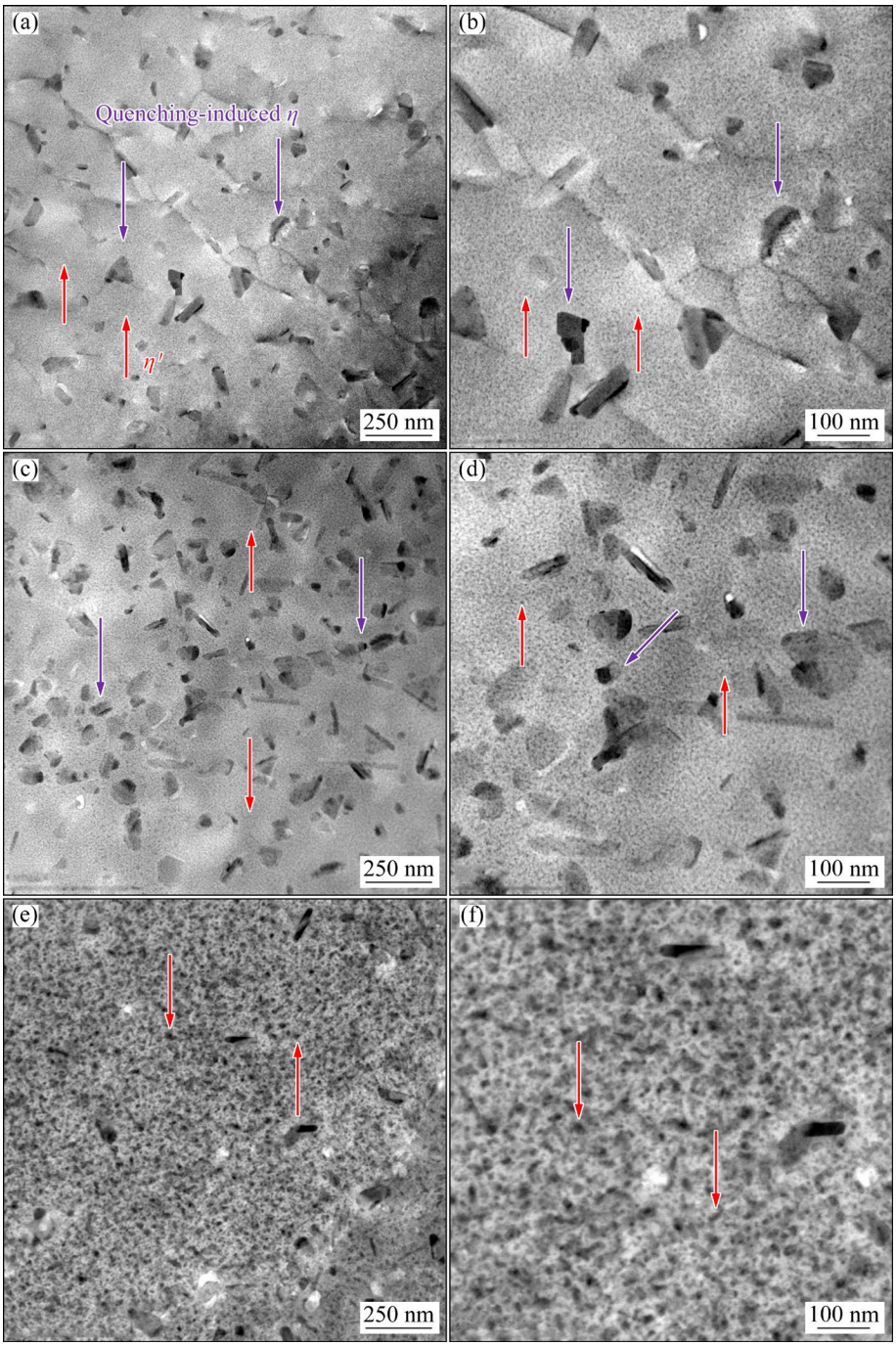

Fig. 2 Bright field TEM images of MPs in 7A75 aluminum alloy: (a, b) T6I4; (c, d) T6I6; (e, f) T6I7

after T6I4 and T6I6 aging treatments, respectively. However, when subjected to T6I7 aging treatment, the morphologies of the MPs significantly differ from that of the T6I4 and T6I6 aging processes, with the MPs growing significantly into a size of approximately 15.7 nm.

Figure 3 displays high angel annular dark field (STEM-HADDF) images and energy dispersive spectroscopy (EDS) analysis of 7A75 aluminum alloy at and around GBPs treated with different interrupted aging methods. Qualitatively, it can be observed from Fig. 3 that Zn, Mg and Cu in the GBPs exhibit noticeable highlighted areas in the energy spectrum when treated with different interrupted aging methods. This indicates that Zn, Mg and Cu have a significant tendency to segregate within the GBPs of the alloy. On the other hand, Fe, Cr and Zr in the GBPs do not exhibit prominent highlighted areas in the energy spectrum, suggesting that they are uniformly distributed within the GBPs. Therefore, it can be concluded that Zn, Mg and Cu exhibit significant segregation within the GBPs of the alloy, while Fe, Cr, and Zr do not.

To facilitate a more clear and intuitive quantitative analysis of element segregation at and around GBPs subjected to different interrupted aging treatments, several GBPs with distinct morphology and evident segregation are selected. These GBPs were then subjected to specific element composition analysis under each interrupted aging temper. The results are presented in Table 4. It is evident that elements in different GBPs exhibit similar degrees of segregation under the same aging process. However, when subjected to different interrupted aging treatments, elements of the same type display significantly different degrees of segregation. For instance, the atomic fraction of Zn in T6I4, T6I6 and T6I7 aging decreases from 9.92% to 8.23% and 6.87%, respectively. Similarly, the atomic fraction of Mg in T6I4, T6I6 and T6I7 aging decreases from 12.66% to 8.43% and 7.00%, respectively. Conversely, the atomic fraction of Cu in T6I4, T6I6 and T6I7 aging increases from 1.83% to 2.47% and 3.41%, respectively. Additionally, the atomic fraction of Fe decreases from 0.13% to 0.05% and 0.05%, while the atomic fraction of Zr decreases from 0.06% to 0.12% and 0.18%.

3.3 Corrosion tests

3.3.1 Intergranular corrosion test

Figure 4 presents the metallographic images and a schematic diagram illustrating the maximum corrosion depth of 7A75 aluminum alloy after immersion in an IGC solution for 6 h, following different interrupted aging treatments. It is evident from that significant IGC characteristic occurs in samples treated with T6I4 aging. The corrosion morphology exhibits a grid pattern and penetrates deeply into the alloy along the grain boundaries, resulting in extensive corrosion damage to the alloy with a maximum corrosion depth of 116.3 μm (Fig. 4(a)). In contrast, samples subjected to T6I6 and T6I7 aging treatments do not exhibit obvious IGC characteristics, as shown in Figs. 4(b) and (c). However, the corrosion morphologies reveal the discontinuous corrosion pits with the maximum corrosion depths of 89.5 and 46.9 μm, respectively. Figure 4(d) provides a schematic diagram illustrating the corrosion depths at different positions of the alloy resulting from the various interrupted aging treatments. The presence of larger grains and flat, elongated grains in the edge of the extruded bar, due to significant grain deformation, renders the alloy more susceptible to local corrosion. Consequently, the corrosion depth distribution indicates that the center of the sample experiences greater corrosion depth compared to the edge [23].

3.3.2 Exfoliation corrosion test

Figure 5 displays the metallographic images of the maximum corrosion depth of 7A75 aluminum alloy after soaking in the EXCO solution for 48 h and being treated with different interrupted aging processes. As shown in Fig. 5, the corrosion has penetrated into the fiber crystal region in the samples treated with T6I4 aging. Due to the stress caused by the corrosion products, some of the fiber crystals have been lifted, resulting in noticeable delamination and peeling phenomena. The maximum corrosion depth in this case is 468.5 μm (Fig. 5(a)). In contrast, in the T6I6 and T6I7 aging processes, there is no evident laminar-peeling phenomenon. Instead, the fiber crystals are corroded and detached from the matrix, forming partially pitting pits of various sizes. The maximum corrosion depths in these cases are 324.3 and 256.9 μm, respectively (Figs. 5(b) and (c)). Figure 5(d)

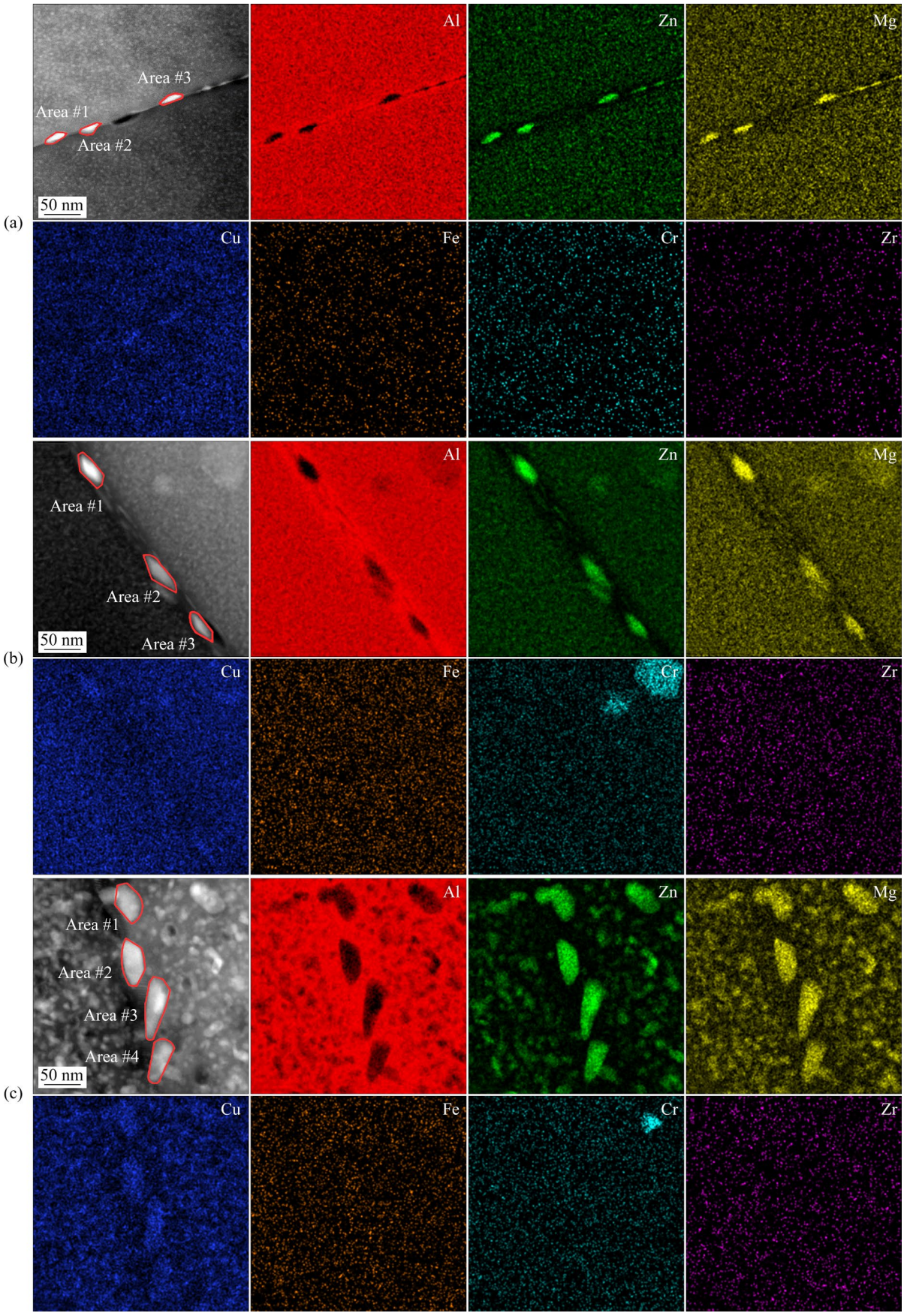

Fig. 3 STEM-HADDF images and EDS analysis at and around GBPs of 7A75 aluminum alloy: (a) T6I4; (b) T6I6; (c) T6I7

Table 4 Segregation results of different elements of 7A75 aluminum alloy treated by different aging treatments (at.%)

Aging treatment	Area No. in Fig. 3	Al	Zn	Mg	Cu	Fe	Cr	Zr
T6I4	1	74.73	10.13	12.88	1.78	0.13	0.04	0.05
	2	74.22	9.73	12.12	1.89	0.12	0.05	0.06
	3	74.14	9.91	12.98	1.82	0.14	0.06	0.07
T6I6	1	80.59	8.32	8.34	2.46	0.06	0.06	0.12
	2	81.11	8.10	8.42	2.48	0.05	0.03	0.12
	3	81.31	8.28	8.53	2.46	0.05	0.05	0.12
T6I7	1	82.38	6.99	6.95	3.40	0.05	0.06	0.17
	2	82.35	6.89	6.97	3.38	0.07	0.05	0.18
	3	82.79	6.73	6.97	3.42	0.03	0.03	0.19
	4	82.00	6.86	7.12	3.42	0.05	0.04	0.17

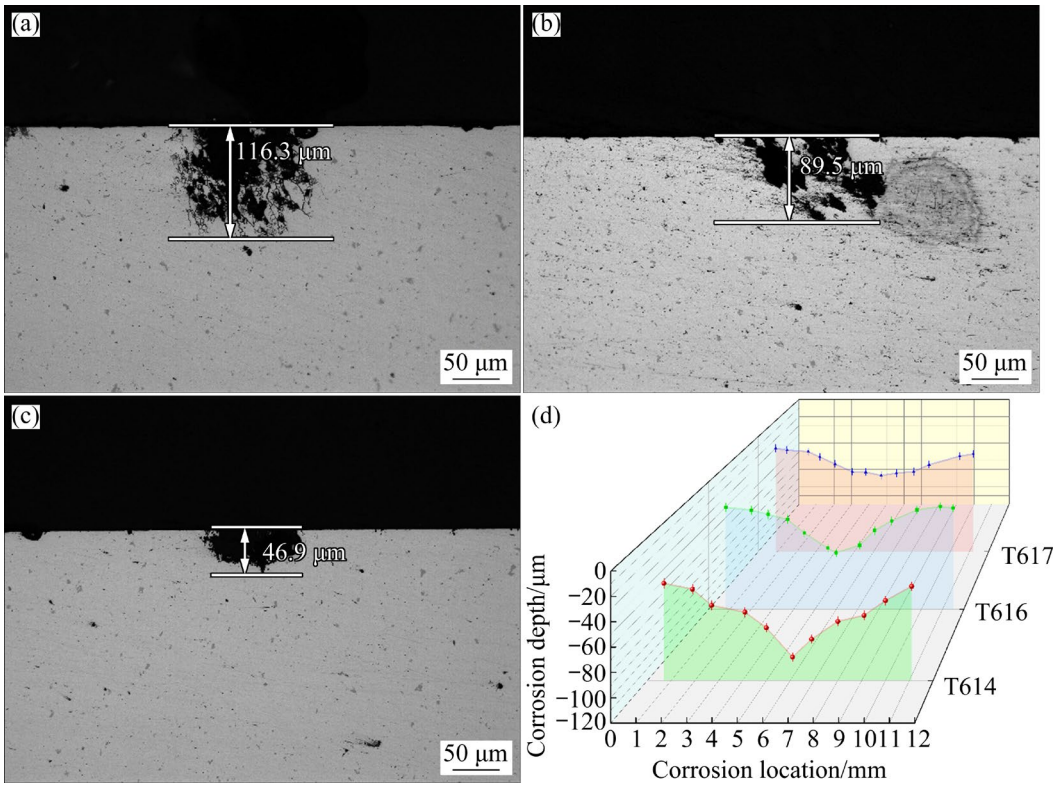

Fig. 4 IGC morphologies of 7A75 aluminum alloy treated by different interrupted aging treatments: (a) T6I4; (b) T6I6; (c) T6I7; (d) Schematic diagram of corrosion depth

presents a schematic diagram illustrating the corrosion depths at different positions of the alloy treated with different interrupted aging processes.

3.3.3 Slow strain rate tensile stress corrosion test

Figure 6 depicts the stress−strain curves of 7A75 aluminum alloy subjected to slow strain rate tensile SCC tests after different interrupted aging treatments. The results of slow strain rate tensile tests are presented in Table 5. Figure 6 and Table 5 demonstrate that the curves for T6I4, T6I6 and T6I7 aging treatments in a 50 °C-3.5 wt.% NaCl solution and 50 °C-silicone oil exhibit the similar trends. They remain consistent primarily in the initial stage of elastic deformation. However, because the Cl^- in NaCl solution has strong corrodibility, it will further erode the aluminum matrix after breaking the oxide film of the alloy, which impacts the mechanical properties of the alloy. Consequently, the strength of the alloy shows some differences in the subsequent stages of elastoplastic deformation and

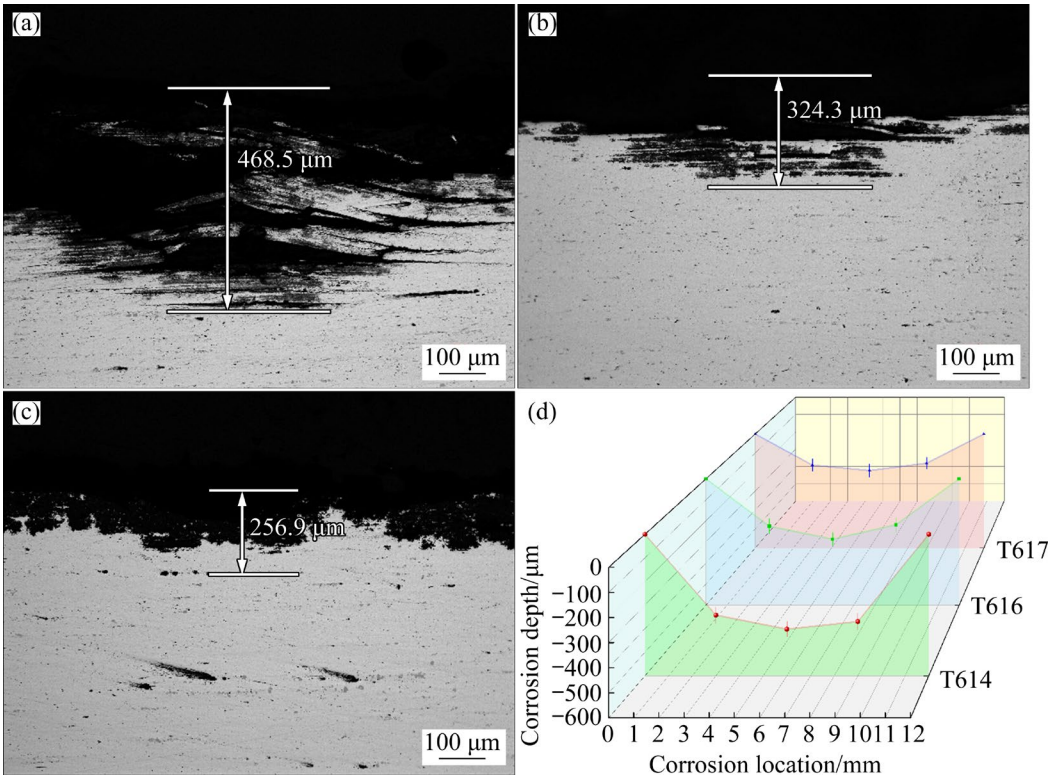

Fig. 5 EXCO morphologies of 7A75 aluminum alloy treated by different interrupted aging treatments: (a) T6I4; (b) T6I6; (c) T6I7; (d) Schematic diagram of corrosion depth

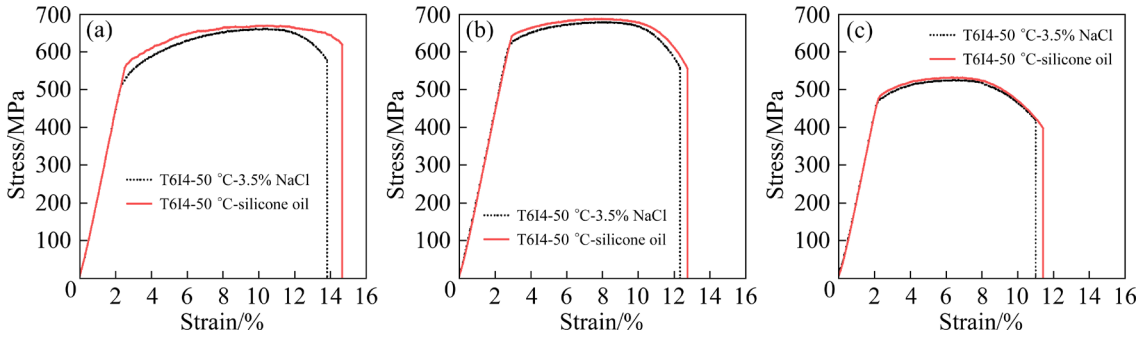

Fig. 6 SCC stress−strain curves of slow strain rate tensile tests of 7A75 aluminum alloy treated by different aging treatments: (a) T6I4; (b) T6I6; (c) T6I7

Table 5 Results of slow strain rate tensile stress corrosion of 7A75 aluminum alloy

Aging treatment	Medium	σ/MPa	δ/%	Strength loss/%	I_{SSRT}/%
T6I4	50 °C-3.5% NaCl	660.6±1.8	13.8±0.2	1.3±0.5	2.1±0.3
	50 °C-silicone oil	669.5±1.7	14.7±0.1		
T6I6	50 °C-3.5% NaCl	679.0±1.3	12.4±0.1	1.3±0.4	1.6±0.3
	50 °C-silicone oil	687.8±1.4	12.8±0.2		
T6I7	50 °C-3.5% NaCl	525.4±1.2	11.0±0.2	1.1±0.4	1.4±0.3
	50 °C-silicone oil	531.2±1.1	11.4±0.1		

fracture, as shown in Fig. 6. Under the three different interrupted aging treatments, the strength and elongation of the alloy in the 50 °C-3.5% NaCl solution are lower than those in the 50 °C-silicone oil, indicating a loss of strength and toughness. The strength losses are 8.9 MPa (1.3%), 8.8 MPa (1.3%)

and 5.8 MPa (1.1%), and the stress corrosion factors (I_{SSRT}) are 2.1%, 1.6% and 1.4% after T6I4, T6I6 and T6I7 aging processes, respectively. A higher I_{SSRT} indicates a greater sensitivity and poorer resistance to SCC. The I_{SSRT} values for the samples treated with T6I6 and T6I7 aging are similar, suggesting that the samples have similar SCC resistance. However, the I_{SSRT} value for the sample after T6I4 aging is higher, indicating relatively poor SCC resistance.

Figure 7 presents SEM images of the slow strain rate tensile corrosion fracture of 7A75 aluminum alloy treated by different interrupted aging processes. As shown in Figs. 7(a, b), the morphologies of the tensile fracture in a 50 °C-3.5% NaCl solution and a 50 °C-silicone oil are significantly different for the alloy treated with T6I4 aging. However, both exhibit obvious intergranular fracture characteristics. The corrosion fracture resulting from the T6I4 aging process shows evident corrosion areas in the 50 °C-3.5% NaCl solution, accompanied by the accumulation of corrosion products forming noticeable corrosion clusters. Additionally, there are apparent microcracks in some areas (Fig. 7(a)). In contrast, the fracture in the T6I4 aging temper does not form apparent microcracks in the 50 °C-silicone oil, but instead produces a large number of tear dimples near the tear ridges (Fig. 7(b)). The morphologies of the fracture in the 50 °C-3.5% NaCl solution and the 50 °C-silicone oil show no significant difference after T6I6 aging treatment (Figs. 7(c, d)). In both cases, a large number of tear ridges and dimples are observed. The type of fracture is a mixed intergranular fracture, and no apparent corrosion area is found in the corrosive medium. After T6I7

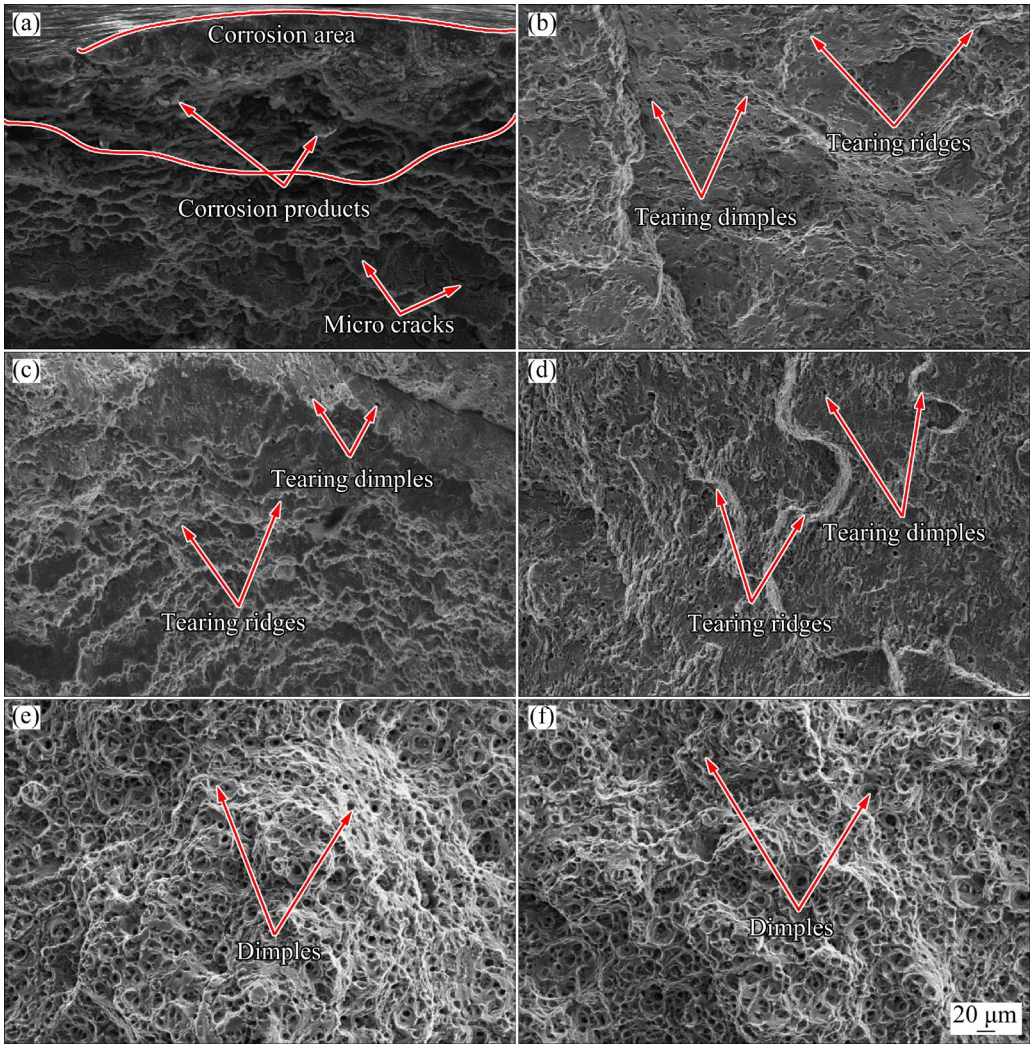

Fig. 7 SEM images of slow strain rate tensile fracture of 7A75 aluminum alloy: (a) T6I4-3.5%NaCl; (b) T6I4-silicone oil; (c) T6I6-3.5%NaCl; (d) T6I6-silicone oil; (e) T6I7-3.5%NaCl; (f) T6I7-silicone oil

aging treatment, there is essentially no difference in the morphologies of the fracture between the 50 °C-3.5% NaCl solution and the 50 °C-silicone oil (Figs. 7(e, f)). In both situations, a large number of dimples can be observed, with sizes of 12.1 and 10.3 μm respectively, indicating obvious transgranular fracture characteristics.

4 Discussion

4.1 Effect of precipitation behavior on mechanical properties

Precipitation strengthening is the primary strengthening mechanism of 7A75 aluminum alloy, which can be strengthened through heat treatment. The behavior of precipitation significantly affects the mechanical properties of the alloy. The primary strengthening phases are coherent GP (I, II) zones and semi-coherent η' precipitates [2,7,25]. During the aging process, the solute concentration in the matrix decreases, reducing the driving force for nucleation [2,26,27]. The rates of nucleation initially increase and then decrease with increasing aging temperature. There is a critical temperature below which the rate of nucleation increases with temperature. Based on the number of previous investigations [28], the aging temperatures used in this experiment are considered to be lower than the critical transition value, and increasing the temperature promotes nucleation and precipitation growth.

The typical η' precipitates are small, spherical or rod-shaped structures. It is widely believed that these precipitates primarily form from GP (I, II) zones, and some of them can also nucleate and grow directly from the matrix, especially at high aging temperature. A lot of researches [29,30] suggest that the metastable η' precipitates have a disk shape at the $\{111\}_{Al}$ plane. During plastic deformation, dislocations slip along the $\{111\}_{Al}$ plane, and only the fine semi-coherent η' metastable precipitates along $\langle 111\rangle_{Al}$ direction can be cut through, effectively impeding the movement of dislocations and providing a strong nail-binding effect. Therefore, fine η' precipitates often exhibit superior strengthening effects. However, larger η precipitates are unable to hinder dislocation movement and instead follow the Orowan bypass mechanism, resulting in a weaker strengthening effect [31−33].

The stage of low-temperature interrupted aging treatments typically involves temperatures below 70 °C for an extended period. This is based on the principle that, at lower temperatures, the critical radius of phase transition decreases, allowing for more stable growth of atomic clusters. This results in the transformation of these clusters into smaller and more dispersed GP (I, II) zones and η' precipitates through prolonged aging treatment, leading to a stronger strengthening effect. The distribution of GBPs and MPs, as observed in TEM images shown in Figs. 1 and 2, is summarized in Fig. 8. When 7A75 aluminum alloy is treated with different interrupted aging processes, there is minimal difference in GBPs between the samples treated with T6I4 and T6I6 aging. However, a small number of coarse η precipitates are formed due to the slow quenching rate. These larger particles contribute relatively less to the strength (Figs. 2(a, b) and Fig. 8(a)). On the other hand, finer and denser dispersed η' precipitates are observed in the matrix (Figs. 2(c, d) and Fig. 8(b)), providing excellent strengthening effects and resulting in tensile strengths of 701.8 and 704.4 MPa, respectively. However, in samples treated with T6I7 aging treatment, the quenching-induced coarse η phases dissolve slowly, and fine second phases gradually grow in the matrix during the re-aging process, forming a coarser discrete matrix structure (Figs. 2(e, f) and Fig. 8(c)). This significantly weakens the strengthening effect, resulting in a tensile strength of only 502.4 MPa.

4.2 Effect of precipitation behavior on local corrosion resistance

The local corrosion resistance of Al−Zn−Mg−Cu alloys preferentially occurs at the grain boundaries and extends deeply into the alloys along these grain boundaries. In a corrosive environment, the η precipitates at the grain boundaries have a more negative potential than the Al matrix, acting as the anode and preferentially dissolving, resulting in corrosion reactions [34,35]. Additionally, the segregation of elements, as well as the sizes and spacings of GBPs, significantly affects the local corrosion resistance of the alloys [36].

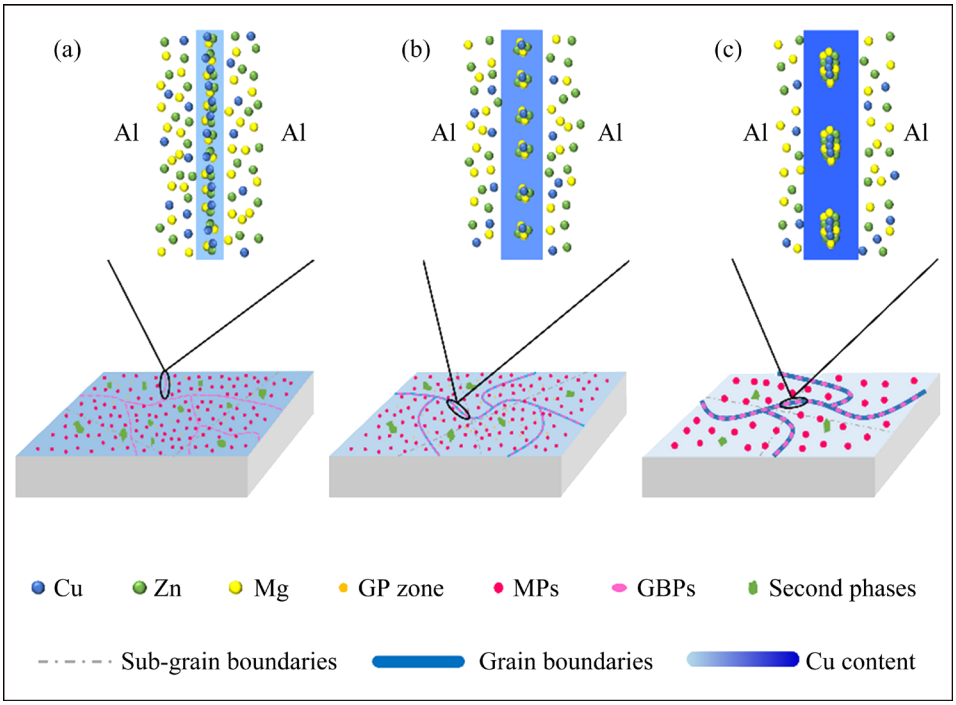

Fig. 8 Schematic diagram of precipitate distribution of 7A75 aluminum alloy treated by different interrupted aging treatments: (a) T6I4; (b) T6I6; (c) T6I7

During the T6I4 aging process, the atomic fractions of Mg, Zn and Cu elements in GBPs are 9.92%, 12.66% and 1.83%, respectively. The GBPs are small and continuously distributed along the grain boundaries. Once local corrosion occurs, it rapidly propagates along the continuous GBPs at the grain boundaries (Figs. 1(b) and 8(a)). Therefore, the local corrosion resistance property is the lowest at the T6I4 aging temper. After T6I6 aging treatment, the atomic fraction of Mg, Zn and Cu in GBPs are 8.23 at.%, 8.43 at.% and 2.47 at.% respectively. When local corrosion occurs, GBPs with larger sizes and spacings can reduce the rate of anodic dissolution at the grain boundaries (Figs. 1(c) and 8(b)) [37]. Therefore, the local corrosion resistance property is improved. After T6I7 aging treatment, the atomic fractions of Mg, Zn and Cu in GBPs are 6.87%, 7.00% and 3.41%, respectively. Coarser and more discontinuous GBPs can disrupt the corrosion channels along the grain boundaries, making it difficult for corrosion to propagate (Figs. 1(d) and 8(c)). Therefore, the local corrosion resistance property of the alloy is the highest at the T6I7 temper.

Although the changes in the contents of various elements in GBPs have a complex effect on the corrosion behavior, it is generally believed that an increase in Zn and Mg content is detrimental to the local corrosion resistance, while an increase in Cu content is beneficial to improving the local corrosion resistance of the alloy [38−40]. From T6I4 to T6I6 and then to T6I7 aging treatments, the increase in Cu and Cr contents and the decrease in Zn, Mg and Fe contents (see Table 4) further reduce the potential difference between GBPs and the Al matrix and greatly improving the local corrosion resistance of the alloy.

4.3 Effect of precipitation behavior on stress corrosion cracking resistance

Al−Zn−Mg−Cu alloys are well-known for their susceptibility to SCC, particularly in corrosive environments containing chloride (Cl^-), bromide (Br^-) and iodide (I^-). Several studies [41−43] have suggested that SCC in these alloys is associated with hydrogen evolution and the segregation of grain boundary elements. Figure 9 illustrates the SCC mechanism in Al−Zn−Mg−Cu alloys. In Fig. 9(a), a passivation film forms on the alloy surface, effectively separating the fresh aluminum matrix from the corrosive medium and inhibiting corrosion. However, prolonged exposure to the

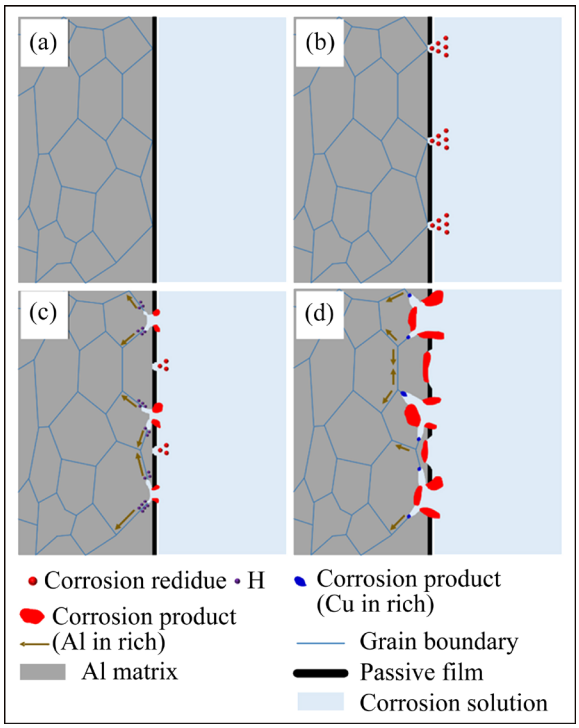

Fig. 9 Schematic diagram of SCC mechanism of 7A75 aluminum alloy: (a) Before corrosion; (b) Early stage of corrosion; (c) Middle stage of corrosion; (d) Late stage of corrosion

corrosive environment causes the chloride ions to erode the passivation film, leading to the formation of corrosive debris and the exposure of the fresh aluminum matrix to the corrosive medium (Fig. 9(b)). This gradual corrosion is facilitated by the increased potential difference between the grain boundaries and the aluminum matrix, which results from the segregation of Zn, Mg, Cu, and other elements at and around the grain boundaries (Fig. 3 and Table 4). At the grain boundaries, the main anodic reactions are represented by Eqs. (1) and (2), while the main cathodic reaction is represented by Eq. (3). These reactions can be expressed as

$$Zn \rightarrow Zn^{2+}+2e \quad (1)$$

$$Mg \rightarrow Mg^{2+}+2e \quad (2)$$

$$2H_2O+2e \rightarrow 2OH^{-}+H_2 \quad (3)$$

Figure 9(c) illustrates the intermediate diagram of SCC. As corrosion progresses, the grain boundaries experience hydrogen evolution reaction accompanied by local alkalization. Figure 9(d) presents a schematic diagram of the late stage of SCC. The dissolution of Zn and Mg in GBPs leads to the formation and accumulation of Cu-rich corrosion products in the grain boundaries, resulting in a higher local corrosion potential. This phenomenon accelerates the SCC of the residual phases surrounding Cu-rich corrosion products and the matrix [44]. As corrosion continues, small pitting pits grow and expand gradually along the grain boundaries, penetrating deeply into the alloy. Under external forces, the micro-cavities also coalesce, forming cracks that eventually lead to the failure of the alloy.

5 Conclusions

(1) The tensile strength of the alloy in T6I7 temper is equivalent to that in T6I4 temper, even exceeding 700 MPa. Additionally, the yield strength is increased by 52.7 MPa to 654.8 MPa. The I_{SSRT} is 1.6%, which is 0.2% higher than T6I7 temper. These results demonstrate that the alloy achieves both high strength and excellent SCC resistance.

(2) The maximum depths of IGC decrease as the aging process progresses, from 116.3 μm in T6I4 to 89.5 μm in T6I6 and further to 46.9 μm in T6I7 aging. Similarly, the maximum depths of EXCO decrease from 468.5 μm in T6I4 to 324.3 μm in T6I6 and further to 256.9 μm in T6I7 after tempering. The I_{SSRT} also decreases from 2.1% in T6I4 to 1.6% in T6I6 and further to 1.4% in T6I7 after tempering.

(3) The sizes of GBPs increase from 5.2 nm in T6I4 to 18.4 nm in T6I6 and further to 32.8 nm in T6I7 aging. Similarly, the sizes of MPs increase from 4.8 nm in T6I4 to 5.7 nm in T6I6 and further to 15.7 nm in T6I7 temper. The atomic fractions of Cu in GBPs also increase from 1.83% in T6I4 to 2.47% in T6I6 and further to 3.41% in T6I7 temper. The sizes of GBPs and MPs, as well as the segregation of elements in GBPs, simultaneously affect the mechanical properties and corrosion resistance of the alloy.

CRediT authorship contribution statement

Xian-wen YANG: Investigations, Formal analysis, Data curation, Writing − Original draft; **Ling-ying YE:** Resources, Supervision; **Yong ZHANG:** Writing − Reviewing & editing; **Quan-shi CHENG:** Data curation, Writing − Reviewing & editing.

Declaration of competing interest

The authors declare that they have no known competing financial interests or personal relationships that could have appeared to influence the work reported in this paper.

Acknowledgments

This work was supported by the Tianjin Key Laboratory of Fastening and Connection Technology Enterprises 2022—2023, China (No. TKLF2022-02-C-02). The authors are thankful for the technical support from the School of Materials Science and Engineering, Central South University, China.

References

[1] CHEN Yan, WEYLAND M, HUTCHINSON C. The effect of interrupted aging on the yield strength and uniform elongation of precipitation-hardened Al alloys [J]. Acta Materialia, 2013, 61(15): 5877−5894.

[2] KE Bin, YE Ling-ying, ZHANG Yong, TANG Jiang-guo, LIU Sheng-dan, LIU Xiao-dong, DONG Yu, WANG Ping. Enhanced mechanical properties and corrosion resistance of an Al−Zn−Mg aluminum alloy through variable-rate non-isothermal aging [J]. Journal of Alloys and Compounds, 2022, 890: 161933.

[3] RANGANATHA R, KUMAR V A, NANDI V S, BHAT R R, MURALIDHARA B K. Multi-stage heat treatment of aluminum alloy AA7049 [J]. Transactions of Nonferrous Metals Society of China, 2013, 23(6): 1570−1575.

[4] MARLAUD T, MALKI B, HENON C, DESCHAMPS A, BAROUX B. Relationship between alloy composition, microstructure and exfoliation corrosion in Al–Zn–Mg–Cu alloys [J]. Corrosion Science, 2011, 53(10): 3139−3149.

[5] SHENG Xiao-fei, HE Cun-xiao, CHENG Ya-juan, RAO Xiao-xiao, HE Guo-ai. New method and mechanism for quickly obtaining quenching sensitivity temperature range of 7055 aluminum alloy [J]. Transactions of Nonferrous Metals Society of China, 2023, 33(01): 36−45.

[6] MARLAUD T, DESCHAMPS A, BLEY F, LEFEBVRE W, BAROUX B. Influence of alloy composition and heat treatment on precipitate composition in Al−Zn−Mg−Cu alloys [J]. Acta Materialia, 2010, 58(1): 248−260.

[7] MACCHI C E, SOMOZA A, DUPASQUIER A, POLMEAR I J. Secondary precipitation in Al−Zn−Mg−(Ag) alloys [J]. Acta Materialia, 2003, 51(17): 5151−5158.

[8] PENG Xiao-yan, GUO Qi, LIANG Xiao-peng, DENG Ying, GU Yi, XU Guo-fu, YIN Zhi-min. Mechanical properties, corrosion behavior and microstructures of a non-isothermal ageing treated Al−Zn−Mg−Cu alloy [J]. Materials Science and Engineering A, 2017, 688: 146−154.

[9] WANG Yun-li, JIANG Hai-chang, LI Zhao-ming, YAN De-sheng, ZHANG Duo, RONG Li-jian. Two-stage double peaks ageing and its effect on stress corrosion cracking susceptibility of Al−Zn−Mg alloy [J]. Journal of Materials Science & Technology, 2018, 34(7): 1250−1257.

[10] LIU Li-li, PAN Qing-lin, WANG Xiang-dong, XIONG Shang-wu. The effects of aging treatments on mechanical property and corrosion behavior of spray formed 7055 aluminium alloy [J]. Journal of Alloys and Compounds, 2018, 735: 261−276.

[11] SPEIDEL M O. Stress corrosion cracking of aluminum alloys [J]. Metallurgical Transactions A, 1975, 6(4): 631−651.

[12] KNIGHT S P, BIRBILIS N, MUDDLE B C, TRUEMAN A R, LYNCH S P. Correlations between intergranular stress corrosion cracking, grain-boundary microchemistry, and grain-boundary electrochemistry for Al−Zn−Mg−Cu alloys [J]. Corrosion Science, 2010, 52(12): 4073−4080.

[13] DENG Ying, YIN Zhi-min, ZHAO Kai, DUAN Jia-qi, HU Jian, HE Zhen-bo. Effects of Sc and Zr microalloying additions and aging time at 120 °C on the corrosion behaviour of an Al−Zn−Mg alloy [J]. Corrosion Science, 2012, 65: 288−298.

[14] XU Dao-kui, BIRBILIS N, ROMETSCH P A. The effect of pre-ageing temperature and retrogression heating rate on the strength and corrosion behaviour of AA7150 [J]. Corrosion Science, 2012, 54: 17−25.

[15] JACUMASSO S C, OLIVEIRA P H F, MARTINS J P, CARVALHO A L M. Microstructural characterization of interrupted aging on an AA7050 aluminum alloy [J]. Materials Characterization, 2019, 152: 180−187.

[16] ANTUNES A M B S, BAPTISTA C A R P, BARBOZA M J R, CARVALHO A L M, MOGILI N V V. Effect of the interrupted aging heat treatment T6I4 on the tensile properties and fatigue resistance of AA7050 alloy [J]. Journal of the Brazilian Society of Mechanical Sciences and Engineering, 2019, 41(8): 319.

[17] LI Jing-feng, PENG Zhuo-wei, LI Chao-xing, JIA Zhi-qiang, CHEN Wen-jing, ZHENG Zi-qiao. Mechanical properties, corrosion behaviors and microstructures of 7075 aluminium alloy with various aging treatments [J]. Transactions of Nonferrous Metals Society of China, 2008, 18(4): 755−762.

[18] KACZMAREK L, STEGLINSKI M, SAWICKI J, BATORY D, KYZIOL K. Optimization of the heat treatment and tribological properties of 2024 and 7075 aluminium alloys [J]. Archives of Metallurgy and Materials, 2013, 58, 535−540.

[19] MA Zhi-min, LIU Jia, LIU Sheng-dan, ZHANG Yong, DENG Yun-lai. Quench-induced contributions of high angle grain boundary and low angle grain boundary to exfoliation corrosion propagation in an AlZnMgCu alloy [J]. Journal of Materials Research and Technology, 2021, 15: 6866−6870.

[20] ZUO Yan, CAO Ling-fei, WU Xiao-dong, WANG Yi-chang, SUN Xuan, SONG Hui, COUPER M J. Effect of ageing temperature on microstructure, mechanical property and corrosion behavior of aluminum alloy 7085 [J]. Journal of Alloys and Compounds, 2020, 823: 153792.

[21] WANG Dang, ZHANG Wen-xue, YI You-ping, HUANG Shi-quan, HE Hai-lin, ZHANG Jing-jing. Influence of retrogression temperature and time on microstructure,

mechanical properties and corrosion behaviors of cryogenically-deformed 7A85 aluminum alloy [J]. Transactions of Nonferrous Metals Society of China, 2024, 334: 392−407.

[22] LIU Sheng-dan, ZHANG Meng-han, LI Qun, SONG Hui, WU Xiang-dong. Effect of quenching rate on strengthening behavior of an Al−Zn−Mg−Cu alloy during natural ageing [J]. Materials Science and Engineering A, 2020, 793: 139900.

[23] HAN Nian-mei, ZHANG Xin-ming, LIU Sheng-dan, KE Bin. Effects of pre-stretching and ageing on the strength and fracture toughness of aluminum alloy 7050 [J]. Materials Science and Engineering A, 2011, 528(10/11): 3714−3721.

[24] LIN Yong-cheng, ZHANG Jing-long, LIU Guan, LIANG Ying-jie. Effects of pre-treatments on aging precipitates and corrosion resistance of a creep-aged Al−Zn−Mg−Cu alloy [J]. Materials & Design, 2015, 83: 866−875.

[25] AARONSON H I, KINSMAN K R, RUSSELL K C. The volume free energy change associated with precipitate nucleation [J]. Scripta Metallurgica, 1970, 4(2): 101−106.

[26] ZHANG Yong-jie, MIYAMOTO G, SHINBO K, FURUHARA T. Weak influence of ferrite growth rate and strong influence of driving force on dispersion of VC interphase precipitation in low carbon steels [J]. Acta Materialia, 2020, 186: 533−544.

[27] MOKSHIN A V, GALIMZYANOV B N, BARRAT J L. Extension of classical nucleation theory for uniformly sheared systems [J]. Physical Review E, 2013, 87(6): 062307.

[28] JIANG Da-ming, LIU Yuan, LIANG Shuai, XIE Wen-long. The effects of non-isothermal aging on the strength and corrosion behavior of Al−Zn−Mg−Cu alloy [J]. Journal of Alloys and Compounds, 2016, 681: 57−65.

[29] CHEN Jun-zhuo, ZHEN Liang, YANG Shuo-jie, SHAO Wen-zhu, DAI Sheng-long. Investigation of precipitation behavior and related hardening in AA 7055 aluminum alloy [J]. Materials Science and Engineering A, 2009, 500(1/2): 34−42.

[30] FENG Chun, LIU Zhi-yi, NING Ai-ling, ZENG Su-ming. Effect of low temperature aging on microstructure and mechanical properties of super-high strength aluminum alloy [J]. Journal of Central South University of Technology, 2006, 13(5): 461−467.

[31] ZHANG Meng-han, LI Cheng-bo, ZHANG Yong, LIU Sheng-dan, JIANG Jing-yu, TANG Jiang-guo. Effect of hot deformation on microstructure and quenching-induced precipitation behavior of Al−Zn−Mg−Cu alloy [J]. Materials Characterization, 2021, 172: 110861.

[32] MOGHADDAM M, ZAREI-HANZAKI A, PISHBIN M H, SHAFIEIZAD A H, OLIVEIRA V B. Characterization of the microstructure, texture and mechanical properties of 7075 aluminum alloy in early stage of severe plastic deformation [J]. Materials Characterization, 2016, 119: 137−147.

[33] YUAN Liang-liang, GUO Ming-xing, ZHANG Ji-shan, ZHUANG Lin-zhong. Synergy in hybrid multi-scale particles for the improved formability of Al−Zn−Mg−Cu alloys [J]. Journal of Materials Research and Technology, 2021, 10: 1143−1157.

[34] SONG Feng-xuan, ZHANG Xin-ming, LIU Sheng-dan, TAN Qi, LI Dong-feng. The effect of quench rate and overageing temper on the corrosion behaviour of AA7050 [J]. Corrosion Science, 2014, 78: 276−286.

[35] KAIRY S K, TURK S, BIRBILIS N, SHEKHTER A. The role of microstructure and microchemistry on intergranular corrosion of aluminium alloy AA7085-T7452 [J]. Corrosion Science, 2018, 143: 414−427.

[36] SUN Xiao-ying, ZHANG Bo, LIN Hua-qiang, ZHOU Yang-tao, SUN Lin, WANG Jian-qiu. Correlations between stress corrosion cracking susceptibility and grain boundary microstructures for an Al−Zn−Mg alloy [J]. Corrosion Science, 2013, 77: 103−112.

[37] WANG Yi-chang, CAO Ling-fei, WU Xiao-dong, TONG Xin, LIAO Bin, HUANG Guang-jie. Effect of retrogression treatments on microstructure, hardness and corrosion behaviors of aluminum alloy 7085 [J]. Journal of Alloys and Compounds, 2020, 814: 152264.

[38] WANG Zhi-xiu, JIANG Hui-hui, LI Hai, LI Song. Effect of solution-treating temperature on the intergranular corrosion of a peak-aged Al−Zn−Mg−Cu alloy [J]. Journal of Materials Research and Technology, 2020, 9(3): 6497−6511.

[39] XIAO Guan-fei, JIANG Ju-fu, WANG Ying, LIU Ying-ze, ZHANG Ying, GUO Bao-yong, HE Zhen, XIAN Xi-rui. Microstructure and mechanical properties of 7075 aluminum alloy parts formed by semi-solid thixoextrusion [J]. Transactions of Nonferrous Metals Society of China, 2023, 33: 3235−3249.

[40] FENG Lei, PAN Qing-lin, WEI Li-li, HUANG Zhi-qi, LIU Zhi-ming. Through-thickness inhomogeneity of localized corrosion in 7050-T7451 Al alloy thick plate [J]. Journal of Central South University, 2015, 22(7): 2423−2434.

[41] ALBRECHT J, THOMPSON A W, BERNSTEIN I M. The role of microstructure in hydrogen-assisted fracture of 7075 aluminum [J]. Metallurgical Transactions A, 1979, 10(11): 1759−1766.

[42] TALIANKER M, CINA B. Retrogression and reaging and the role of dislocations in the stress corrosion of 7000-type aluminum alloys [J]. Metallurgical Transactions A, 1989, 20(10): 2087−2092.

[43] UMAMAHESHWER RAO A C, VASU V, GOVINDARAJU M, SAI SRINADH K V. Stress corrosion cracking behaviour of 7xxx aluminum alloys: A literature review [J]. Transactions of Nonferrous Metals Society of China, 2016, 26(6): 1447−1471.

[44] JIANG Lei, ZHANG Zhi-hao, FU Hua-dong, HUANG Shi-yu, ZHUANG Da-wei, XIE Jian-xin. Corrosion behavior and mechanism of Al−Zn−Mg−Cu alloy based on the characterization of the secondary phases [J]. Materials Characterization, 2022, 189: 111974.

断续时效对 7A75 铝合金力学性能和抗腐蚀性能的影响

杨献文[1]，叶凌英[1]，张 勇[1]，程全士[1,2]

1. 中南大学 材料科学与工程学院，长沙 410083；
2. 航天精工股份有限公司，天津 300300

摘 要：通过电导率、力学性能、局部腐蚀性能和慢应变速率拉伸应力腐蚀等性能测试，结合金相显微镜、扫描电子显微镜(SEM)和透射电子显微镜(TEM)等显微组织表征方法，研究不同断续时效工艺对 7A75 铝合金挤压棒材力学性能和抗腐蚀性能的影响。结果表明：合金经 T6I6 处理后，其抗拉强度与 T6I4 时效合金的相当，甚至超过 700 MPa，屈服强度提高了 52.7 MPa，达到 654.8 MPa；最大晶间腐蚀和剥落腐蚀深度分别从 116.3 和 468.5 μm 下降至 89.5 和 324.3 μm；应变腐蚀因子从 2.1%下降至 1.6%。同时获得了高强度与高耐应力腐蚀开裂性能。同样，当合金经 T6I4、T6I6 和 T6I7 处理后，晶界析出相的尺寸分别为 5.2、18.4 和 32.8 nm，基体析出相的尺寸分别为 4.8、5.7 和 15.7 nm；晶界析出相中 Zn 的原子分数分别为 9.92%、8.23%和 6.87%，Mg 的原子分数分别为 12.66%、8.43%和 7.00%；Cu 的原子分数分别为 1.83%、2.47%和 3.41%。

关键词：7A75 铝合金；断续时效；时效析出行为；力学性能；晶间腐蚀；剥落腐蚀；应力腐蚀开裂

(Edited by Xiang-qun LI)